Fiske modes and Eck steps in long Josephson junctions: Theory and experiments

M. Cirillo
Dipartimento di Fisica and Unità INFM, Università di Roma ''Tor Vergata,'' I-00133 Roma, Italy

N. Grønbech-Jensen and M. R. Samuelsen*
Theoretical Division, Los Alamos National Laboratory, Los Alamos, New Mexico 87545

M. Salerno
Dipartimento di Scienze Fisiche ''E. R. Caianiello'' and Unità INFM, Università di Salerno, I-84100 Salerno, Italy

G. Verona Rinati
Dipartimento di Scienze e Tecnologie Fisiche ed Energetiche, Università di Roma ''Tor Vergata,'' I-00133 Roma, Italy
(Received 21 January 1998; revised manuscript received 1 June 1998)

We report on a systematic investigation of the properties of long Josephson junctions under the application of magnetic fields generating Fiske and Eck steps in the current-voltage characteristics. Numerical data and experimental results are compared with a cavity mode-based model predicting the voltage position and the amplitude of the current singularities. The comparison shows that this model can account for the shape and for the maximum current modulation of the singularities when the field penetration overcomes Meissner shielding above the value $H_0=2\lambda_j j_c$. [S0163-1829(98)05342-9]

I. INTRODUCTION

The excitations of a Josephson junction in the presence of boundary currents generated by an external magnetic field have been investigated by several authors during the past years.[1] In most cases the analysis was performed modeling junctions whose physical dimensions were small compared to the Josephson penetration depth $\lambda_j=\sqrt{\Phi_0/2\pi\mu_0 d j_c}$, $\Phi_0=2.07\times10^{-15}$ Wb being the magnetic flux quantum, $d=\lambda_1+\lambda_2+t$ the magnetic thickness of the junction, and j_c the maximum Josephson current density. Excellent agreement was found in this case between the shape and amplitudes of the current singularities called Fiske steps (FS's) and the proposed models based on the interaction between single-mode cavity waves and the Josephson effect.[2]

Defining L as the physical length of the junction, it is known that, in the very long Josephson junction limit, i.e., $l=L/\lambda_j\gg1$, the junctions exhibit different types of oscillations and complex nonlinear behavior[1] ranging from fluxon shuttling oscillations to spatio-temporal chaos and cavity mode interaction with the Josephson effect. At present, considering only the dc-current-biased junction case, there exist basically two kind of oscillations that justify important features of the current-voltage characteristics: fluxon oscillations and cavity mode interaction with the ac Josephson effect. Fluxon perturbation theory[3] has provided sufficient information and experimental data fitting for the current singularities, called zero-field steps (ZFS's) generated by the shuttling of particlelike flux quanta along the extended dimension of the junction.[4] Multimode expansion was also employed[5] in order to account for experimental features regarding ZFS's in intermediate-length junctions. This analysis showed that, when the junctions are not very long, most of the dynamics, including fluxon oscillations, can be explained by multimode expansion of the phase difference. The multimode analysis also showed that a wave description becomes inadequate when the normalized length $l\gg1$.

In the present paper we show that even in the very long junction limit the two oscillating regimes, fluxon oscillations and cavity mode resonances (generating Fiske steps), are clearly separated due to the response of the sine-Gordon system to an applied magnetic field. The particlelike behavior is a reliable model when the applied magnetic field is very close to zero. However, if the value of the external magnetic field is above the critical value $H_0=2\lambda_j j_c$, the response of the long junction presents strong evidence of single-mode cavity-wave oscillatory behavior.[6] We investigate quantitatively the features of the current-voltage characteristics of the junctions by numerical simulation and experiments when the applied magnetic field is above this critical value. The data are compared with a single-mode excitation model whose application is justified by the complete field penetration in the junction.

In the next section we present a theoretical extension of the early theories of Fiske modes and the Eck step in Josephson junctions and justify the application to the physical conditions that we will be considering. In Sec. III we compare the theoretical results with numerical data. In Sec. IV we compare the theory with the experimental results obtained with junctions of different lengths and geometries; in Sec. V we summarize the paper.

II. THEORETICAL MODEL

We take as a starting point the perturbed sine-Gordon equation

$$\phi_{tt}-\phi_{xx}+\alpha\phi_t+\sin\phi=\eta, \tag{1}$$

with the boundary conditions

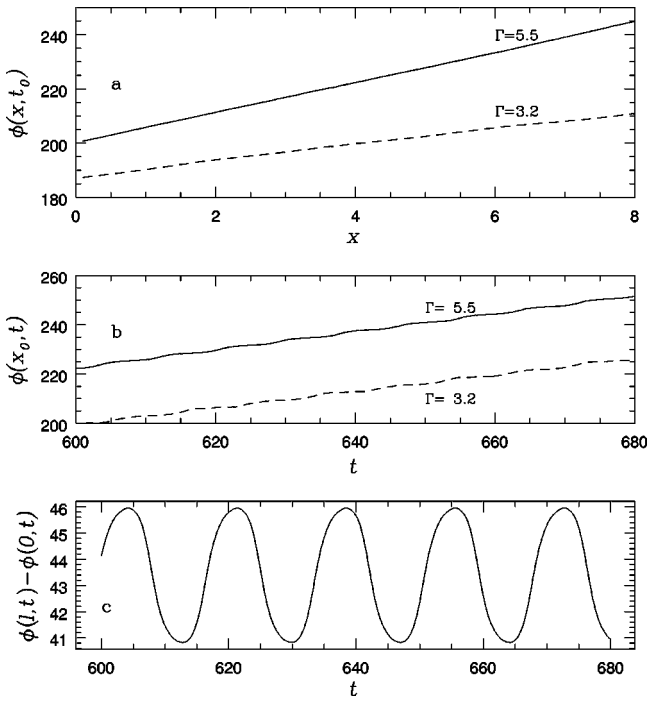

FIG. 1. Results of numerical integration of the driven sine-Gordon system [Eqs. (1) and (2)] for $l=8$, $\eta=0.06$, and $\alpha=0.1$. (a) Phase configuration along the junction for different values of the normalized external magnetic field Γ. (b) Time dependence of the voltage in the middle of the junction. (c) Evolution of the phase difference between the ends of the junction for $\Gamma=5.5$.

$$\phi_x(t,0)=\phi_x(t,l)=\Gamma. \tag{2}$$

In Eq. (1), η is the dc-bias current normalized to the maximum critical current I_c, and $\alpha=1/\sqrt{\beta_c}$ is the damping coefficient with $\beta_c=2\pi I_c R^2 C/\Phi_0$ denoting the McCumber parameter[2] (R is the resistance in the subgap region and C the total capacitance of the junction). In the system (1) and (2) distances are measured with respect to λ_j and time with respect to the reciprocal Josephson plasma frequency ω_j^{-1}, $\omega_j=\sqrt{2\pi j_c/\Phi_0 C}$. We remark that assuming a constant value for R is an approximation whose validity depends on the amplitude of the voltage interval that we consider in the subgap region; this limitation must be considered when trying to use the model, Eqs. (1) and (2), over large voltage ranges. In Eq. (2), $\Gamma=H_e/\lambda_j j_c$ is the normalized external magnetic field. It is evident from the position of our problem that we neglect two-dimensional effects: only one dimension of the rectangular junctions that we model can be larger than λ_j.

It is known from experiments, numerical simulations, and low-temperature scanning electron microscope (LTSEM) imaging[6] that stable Fiske steps appear in the current-voltage characteristics of long Josephson junctions when $\Gamma>2$. As a starting point of our analysis we show that, when this condition is satisfied, the phase difference along the spatial interval, at time t, can be written as

$$\phi(x,t)\approx\omega t+\Gamma x, \tag{3}$$

where $\omega=\langle V\rangle$ is defined by the fundamental Josephson relation in the units of the system (1) and (2). In Fig. 1 we display the result of a numerical integration of the system (1) and (2) performed for flat initial conditions ($\phi=0=\phi_t$ for every point in space) and parameter values $l=8$, $\eta=0.06$, and $\alpha=0.1$. All the results of the integration were taken after allowing the decaying of the initial transients (typically several thousand integration time steps). In Fig. 1(a) we plot the dependence of the phase along the normalized spatial interval at $t=600$ for two values of the parameter Γ which are, respectively, 3.2 and 5.5 as indicated by the labels. From this plot we find that the phase has an overall linear dependence on the spatial coordinate and the slope of the straight lines, as obtained from a linear interpolation, is 2.9 and 5.5, respectively, for $\Gamma=3.2$ and $\Gamma=5.5$, meaning that the ansatz (3) becomes better when increasing the value of the external field.

In Fig. 1(b) instead, we show the time dependence of the phase in the center section of the numerical model ($x_0=4$) for the same two values of the external magnetic field. In this case the linear fitting of the two curves gives a slope equal, respectively, to 0.335 ($\Gamma=3.2$) and 0.367 ($\Gamma=5.5$); we note that these two values obtained from the fit are equal, within less than 0.1%, to the average voltage $\langle V\rangle=\omega$ evaluated directly averaging the numerical data. Figures 1(a) and 1(b) demonstrate that our Eq. (3) represents a reasonable starting point for the analysis of the dynamics of the junction.

However, in Fig. 1(b) we see that, on time scales of the order of $1/\omega$, there are regular oscillations of the phase that are not accounted for in Eq. (3). The overall effect (and the amplitude) of these spatial oscillations is epitomized in Fig. 1(c) where we plot the time dependence of the phase difference between the end sections of the junction model $\Delta\phi(t)=\phi(l,t)-\phi(0,t)$. We see that this variable has a regular oscillation [parameters here are the same as if Fig. 1(a) and 1(b) with $\Gamma=5.5$] and excursions of the order of 5 around the value 43.5 which is essentially the flux linked to the junction ($\Gamma l=44$). The kind of dependences that we observe in Figs. 1(b) and 1(c) gives us an indication that the overall time increase of the phase along the junction takes place while the phase difference between the two ends oscillates periodically, just like in a cavity mode excitation. Indeed the average voltages of Fig. 1(b) and the angular frequency of the oscillation of Fig. 1(c) are close to π/l which is the normalized frequency of the first mode of a cavity with length l.

In the particular case of Fig. 1 the excitation drives the junction on the first Fiske step of the current-voltage characteristics. In terms of real junctions this means that we would be biased at the voltage $v_n=n\Phi_0\bar{c}/2L$ with the step order number $n=1$; here $\bar{c}$ is the speed of light in the oxide barrier (typically a few percent of the free-space velocity).

The above observations suggest that Eq. (3) can be completed with a time dependence which accounts for the spatial perturbations in the form of a linear cavity mode expansion whose spatial periodicity is determined by the multiples of $\omega=\pi/l$. Our starting point for the development of the theoretical analysis is the following modification of Eq. (3):

$$\phi(x,t)=\omega t+\Gamma x+\psi(x,t), \tag{4}$$

with $|\psi(x,t)|\ll 1$.

We will derive the equations for the current-voltage characteristics associated with FS's substituting Eq. (4) in the system (1) and (2), imposing a classical cavity mode expansion for the function $\psi(x,t)$. It is worth noting that Eq. (4) was the starting point for an early analysis of the interaction of cavity waves with the Josephson effect.[7–9] The analysis of the FS's was performed on the basis of Eq. (4) in the limit $\lambda_j \to \infty$, a condition that would guarantee the negligible effect of the $\sin\phi$ nonlinear term in Eq. (1). This restriction, however, does not constitute a necessary condition for the applicability of the ansatz (4). The simplest form of (dynamic) solution in the form of Eq. (4) for the system (1) and (2) is represented by the solution for which the function $\psi(x,t)$ of Eq. (4) has a constant (time and space independent) value, i.e.,

$$\phi_0 = \omega t + \Gamma x + \theta_0, \tag{5}$$

where θ_0 is an arbitrary phase and ω is determined by the power balance condition $\omega = \eta/\alpha$. For this solution the nonlinear term in Eq. (1) is zero (on average) and the system reduces to a linear one. We expand now the general solution of Eq. (1) as $\phi = \phi_0 + \psi$ which gives the linear equation

$$\psi_{xx} - \psi_{tt} = \sin\phi_0 + \cos\phi_0\psi + \alpha\psi_t - \eta + \alpha\omega, \tag{6}$$

with the boundary conditions

$$\psi_x(0,t) = \psi_x(l,t) = 0. \tag{7}$$

Solutions to Eq. (6), fulfilling the boundary conditions (7), can be obtained as

$$\psi = \sum_{n=0}^{\infty} (A_n \cos\omega t + B_n \sin\omega t)\cos k_n x, \tag{8}$$

where $k_n = n\pi/l$. Inserting Eq. (8) into Eq. (6), multiplying by $\cos k_j x$, and integrating over the length of the junction, we get by separating $\cos\omega t$ and $\sin\omega t$ terms the following form for the coefficients A_n and B_n:

$$A_n = -\frac{2\Gamma l\{(\omega^2 - k_n^2)[1-(-1)^n\cos\Gamma l] + \alpha\omega(-1)^n\sin\Gamma l\}}{(1+\delta_{n,0})[(k_n l)^2 - (\Gamma l)^2][(\omega^2-k_n^2)^2 + \alpha^2\omega^2]}, \tag{9}$$

$$B_n = -\frac{2\Gamma l\{(\omega^2 - k_n^2)(-1)^n\sin\Gamma l - \alpha\omega[1-(-1)^n\cos\Gamma l]\}}{(1+\delta_{n,0})[(k_n l)^2 - (\Gamma l)^2][(\omega^2-k_n^2)^2 + \alpha^2\omega^2]}. \tag{10}$$

The current-voltage characteristics follow from the dc part of Eq. (6) as

$$\overline{\langle\cos\phi_0\psi\rangle} = +\eta - \alpha\omega, \tag{11}$$

where the average on the left hand side is performed over space and time variables. The explicit calculations show that

$$\eta = \alpha\omega + \sum_{n=-\infty}^{\infty} \frac{1}{2} \frac{\left(\frac{\Gamma l}{2}\right)^2}{\left(\frac{\Gamma l + k_n l}{2}\right)^2} \frac{\sin^2\frac{\Gamma l - k_n l}{2}}{\left(\frac{\Gamma l - k_n l}{2}\right)^2} \frac{\alpha\omega}{(\omega^2 - k_n^2)^2 + \alpha^2\omega^2}. \tag{12}$$

The first term in Eq. (12) represents the Ohmic part of the current-voltage characteristics; the second term gives an infinite series of equidistant resonances of width α. The distance between these resonances is π/l. Note that this is the normalized frequency spacing between the resonances. Recalling that the frequency is normalized to ω_j and that $\bar{c} = \omega_j\lambda_j$ we recover the classical expression for the frequency spacing of the resonances determined by $\bar{c}/2l$. The height of the resonances is modulated by a slowly varying amplitude factor and a fast (Fraunhofer) amplitude factor. The maximum of each resonance is $1/\alpha\omega$. The Fraunhofer factor emphasizes the resonance closest to $\omega = \Gamma$ and drops off fast: typically only two or three resonances produce significant current. If Γl is an even multiple of π, the odd numbered resonances prevail except for the central resonance, and if Γl is an odd multiple of π, the even numbered resonances prevail except, again, for the central resonance. The slow varying factor (including the $\frac{1}{2}$) has its maximum ($\frac{1}{2}$) for the resonance at $k_n = 0$, and drops down to $\frac{1}{8}$ for the resonance at $k_n = \Gamma$. Note that in the limit of infinite length only modes around $k_n = \pm\Gamma$ contribute, this leading to

$$\eta = \alpha\omega + \frac{1}{2}\frac{\alpha\omega}{(\omega^2 - \Gamma^2)^2 + \alpha^2\omega^2}, \tag{13}$$

which is exactly the expression of Eck, Scalapino, and Taylor[8] for the Eck step (ES). Their quality factor Q is in our case the ratio ω/α. Note that the width of the resonances expressed by Eq. (12) is α while their separation is π/l. Thus, as long as $\alpha l \ll \pi$, there is a clear separation of the FS's while it shall be surely difficult to observe distinctions between them in the opposite case ($\alpha l \gg \pi$).

III. NUMERICAL RESULTS: COMPARISON WITH THEORY

We will compare first the theoretical predictions with numerical results that we have obtained for the maximum height of the first FS's as a function of the external magnetic field. This can be done from Eq. (12) by setting for the nth resonance $\omega = n/\pi l$. The numerical results were performed integrating the system (1) and (2) by a standard finite difference method in time and space.[9] We have numerically evaluated the height of the first Fiske steps for normalized lengths ranging from 0.1 to 8 and the results of the integration (circles) are shown in Fig. 2. Superimposed on the circles we have reported the predictions of Eq. (12) represented by the solid line obtained for $\omega = \pi/l$. Beside imposing this resonant condition for the frequency no fitting parameters were used for any of the data shown in Fig. 2. As a general trend we see from these figures that the agreement between the theoretical model and the simulations tends to be better for

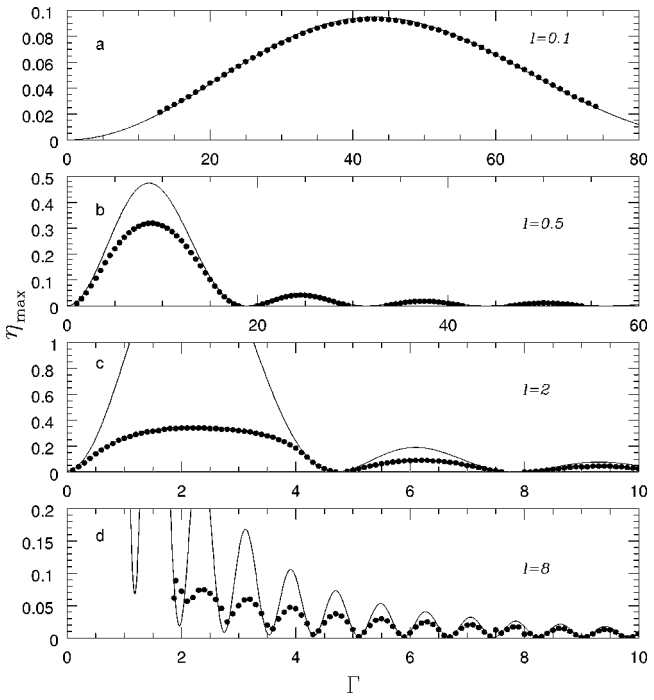

FIG. 2. The numerical (dots) and theoretical (solid line) magnetic field dependence of the current amplitude of the first Fiske step for junctions of lengths (a) 0.1, (b) 0.5, (c) 2, and (d) 8 for a loss parameter $\alpha=0.1$.

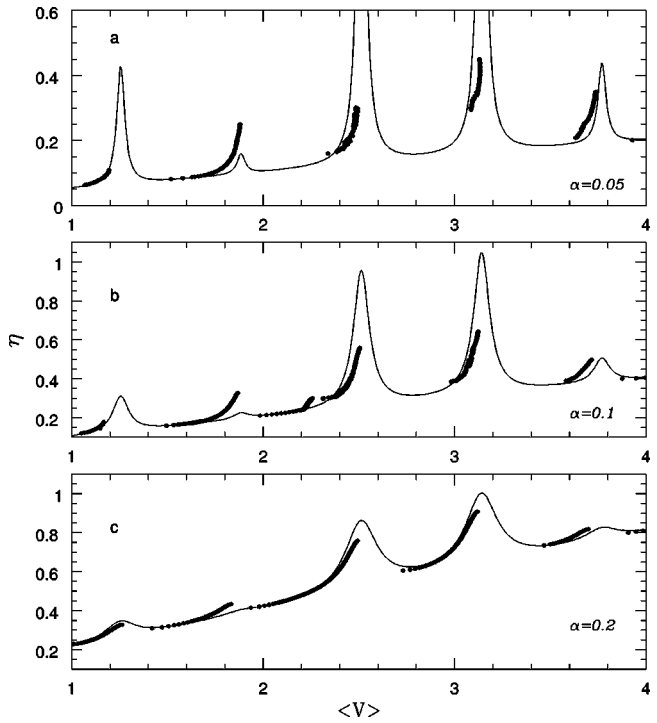

FIG. 3. Current-voltage characteristics obtained fixing the normalized length to $l=5$, $\Gamma=3$ and varying the value of the loss parameter whose value as indicated by the labels in (a), (b), and (c). The dots are the results of the numerical integration and the solid line the theoretical results.

increasing values of the magnetic field which can be expected as the starting approximation, Eq. (4), has physical sense, for junctions having $l>1$, when $\Gamma>2$, and gets better for increasing values of the field. Moving toward the Kulik theory approximation[7] ($\lambda_j\to\infty$) we see in Fig. 2(a) that our model can fit well even the amplitude of the first lobe of the Fiske step. In all cases the periodicity of the modulations is exactly the one indicated by our model, meaning that our cavity-wave analysis is adequate.

We have also simulated current-voltage (I-V) characteristics for fixed values of the magnetic field which represents a somewhat complementary aspect of the diffraction pattern plot. The results of these numerical integrations are reported in Figs. 3–5. In all these figures the numerically obtained I-V curves are represented by the dots while the results of Eq. (12) are represented by solid lines.

In Fig. 3 we show three I-V curves obtained for $l=5$, $\Gamma=3$, and three values of the loss parameter α [respectively, 0.05 (a), 0.1 (b), and 0.2 (c)]. In Fig. 4, we display in the same order with respect to increasing values of $\alpha=0.1$, $\alpha=0.2$, and $\alpha=0.3$ the I-V curves for $l=10$ and $\Gamma=3$. In Figs. 3–5, like in Fig. 2, no fitting parameters were used in order to match numerical experiments and theory. As general trend in these two figures we see that instabilities are present on the steps for lower voltages and lower damping parameters. Instabilities of the Fiske modes for magnetic fields close to the critical value $\Gamma=2$ have been observed previously.[6] When the spurious oscillations are damped out (by increasing α), we see that our model gives a better fit of the numerical data even for values of the field of the order of 2.

By further increasing the loss we reach the parameter-space region where it is not possible to distinguish reso-

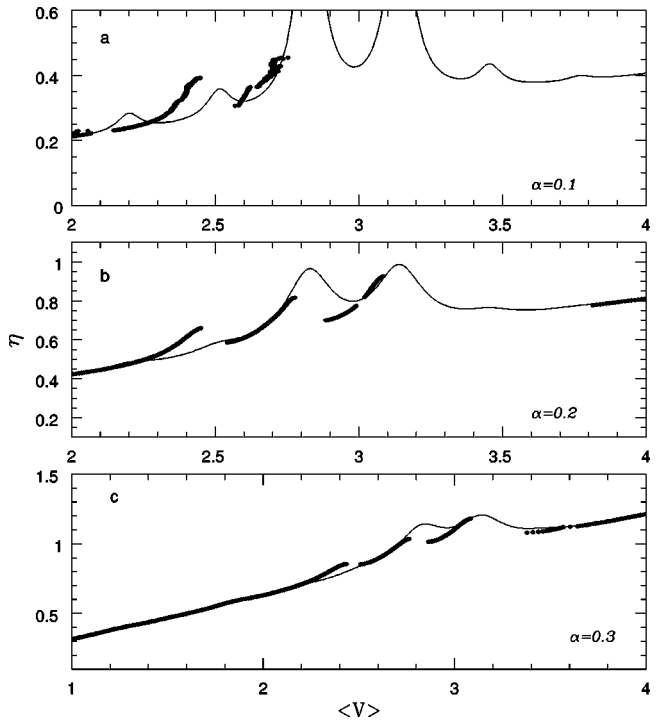

FIG. 4. Numerically evaluated current-voltage characteristics (dots) and theoretical predictions, based on Eq. (12). (a), (b), and (c) are relative to a normalized length $l=10$ and $\Gamma=3$. The labels indicate the value of the loss parameter α.

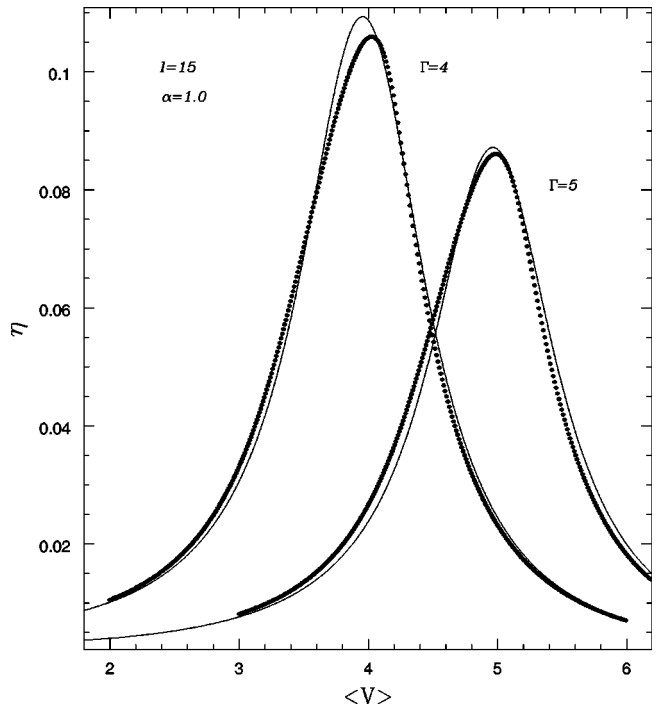

FIG. 5. The current-voltage characteristic of a junction having $l=15$ from the numerical (dots) and theoretical point of view for two different values of the applied field and a loss parameter $\alpha=1.0$. We are in a parameter plane region in which all the FS's merge in a single singularity (the Eck step) whose voltage, for a fixed current, depends linearly upon the value of the external magnetic field.

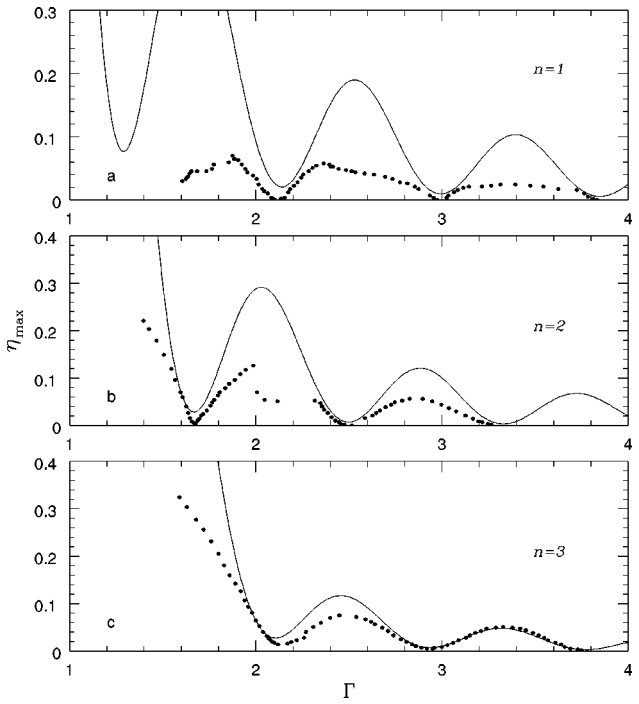

FIG. 6. The experimental modulation pattern (dots) of the first three Fiske steps for an overlap junction having a normalized length $l=7.5$. (a), (b), and (c) represent, respectively, the first, second, and third steps. The value of the loss parameter that gives the best fit is $\alpha=0.15$.

nances anymore and we can observe only a smooth and continuous singularity. An example of this phenomenon is shown in Fig. 5 where we display the results of two numerical integrations for a junction having a length $l=15$ and a loss factor $\alpha=1.0$ for increasing values of the magnetic field Γ. The theory (solid line) is derived directly from Eq. (12). In this picture, however, we have subtracted the Ohmic contribution. Due to the relatively high value of the loss parameter in this case, we can see very clearly the ''resonant'' nature of the Eck step since it is possible to trace the negative resistance part of the curve. The length of the junction and the relatively high value of the voltage can even allow a good fit by using Eq. (13) (in this case the result of the theory would exhibit very slight differences from the theoretical curves shown in Fig. 5).

IV. EXPERIMENTS

We have measured the *I-V* curves of several Nb-NbOx-PbAuIn junctions fabricated according to standard procedures.[10] All the samples had good current-voltage (*I-V*) curves, current densities ranging in the interval (100–3000) A/cm^2, and two basic types of geometries, namely, overlap and in line. We will see, however, that the comparison of our theoretical model with the experiments is not much dependent on the geometry. As for the numerical experiments, we will show first the results of the modulations of the currents with the applied magnetic field and then the current-voltage characteristics.

In Fig. 6 we show the modulations of the currents of the first, second, and third FS's of an overlap[2] junction having a normalized length $l=7.5$. In the figure the currents on the vertical axis are normalized to the maximum Josephson supercurrent of 5.7 mA. The curves in the figure have been obtained for damping parameters α equal, respectively, to $0.15(n=1)$, $0.1(n=2)$, and $0.15(n=3)$. We note that, since the plasma frequency for the junctions under consideration here is of the order of 70 GHz, the voltage of the first step is below the corresponding voltage for which the modulations are more irregular while the voltage of the third step is well above the plasma frequency (this step had an asymptotic voltage of 560 μV). We also see that the modulations appear above $\Gamma\cong 2$ and that the current height gets closer to the expected theoretical value, increasing the step order number. This is a general feature observed in experiments that is due to the fact that below or about the plasma frequency the nonlinearities of the system (1) and (2) may have a strong effect on our linearized model for the Fiske steps.

In Fig. 7 we show the modulations of the first three FS's of an overlap junction having a normalized length $l=15.3$. In this case the value of the loss parameter was 0.05 for $n=1$, and 0.1 for $n=2,3$. Even in this case Eq. (12) explains very well the periodicity of the modulations; also we see that, increasing the step order number, the heights of the steps are fitted better. This result is somewhat expected since increasing the step corresponds to moving away from the plasma frequency of the junction and to decreasing the relative weight of spurious nonlinear oscillations.

Another point in favor of the above argument comes from the results that we have obtained from an in-line junction, shown in Fig. 8. This junction had the same current density

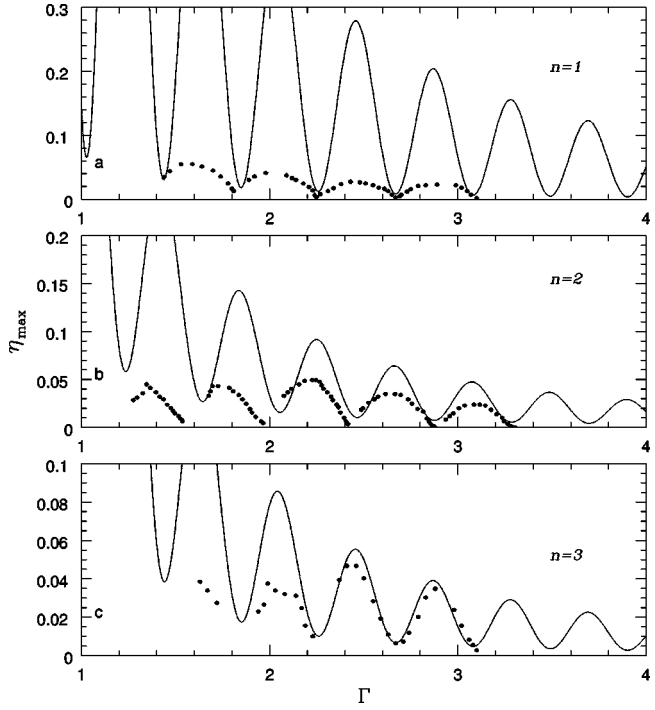

FIG. 7. Modulation plots for a junction having $l=15.3$. The dots are the experimental results and the solid line obtained for the first Fiske step (a) with $\alpha=0.05$, and the second (b) and third (c) with $\alpha=0.1$.

but a smaller normalized length $l=7$ due to a physical length of 50 μm. In this case the asymptotic frequency of the steps was safely above the plasma frequency. The fittings of the current modulations of Fig. 7 were obtained for $\alpha=0.15$. We

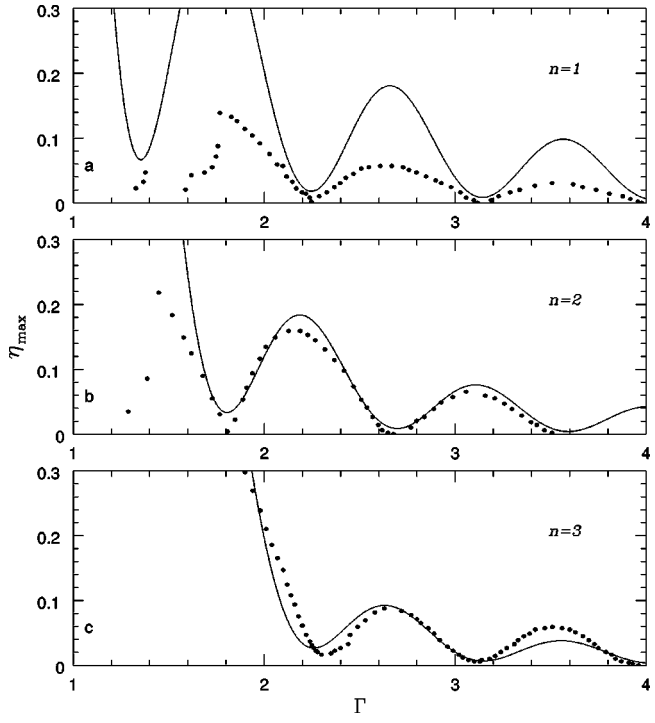

FIG. 8. Experimental data (dots) and theoretical dependences for the first three Fiske steps, respectively. (a), (b), and (c) of an in-line junction having $l=7$. Even in this case the value of the loss parameter that gives the best fit is $\alpha=0.15$.

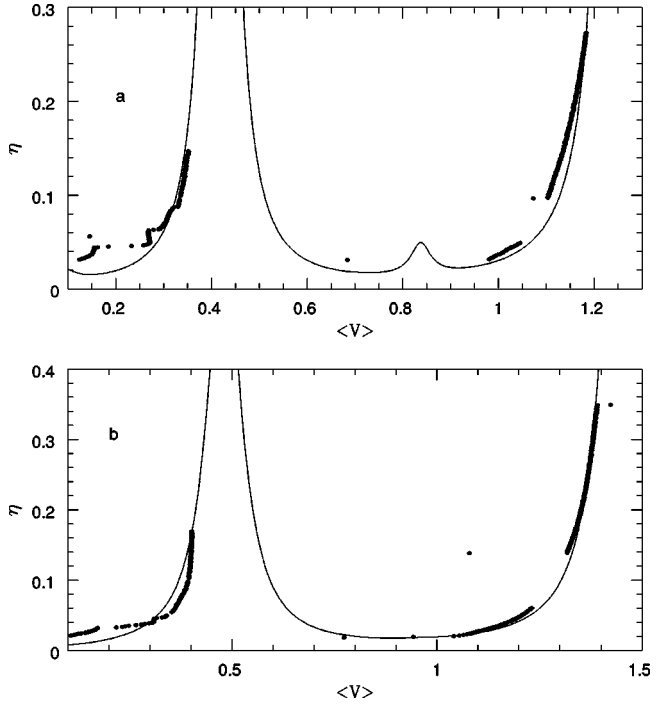

FIG. 9. (a) Current-voltage characteristics of an overlap junction having $l=7.5$ showing the first and third Fiske steps (dots are experimental points). The theoretical curve, obtained on the basis of Eq. (12), is represented by the solid line; the value of the loss factor for the fit was $\alpha=0.05$ and the magnetic field $\Gamma=1.63$. (b) Same as in (a) for the in-line junction having $l=7$: the fit is obtained here for $\alpha=0.1$ and $\Gamma=1.95$.

see that our model is not sensitive to the geometrical configuration of the junction inasmuch as it is based on the total penetration of the field above the critical value $\Gamma=2$. Thus, Eq. (12) can be used even for in-line geometry junctions when the value of the applied magnetic field is above the critical value.

The complementary aspect of Fig. 6 and Fig. 8 is shown in Fig. 9 where we see in (a) the theoretical current-voltage characteristic of the overlap junction obtained for $l=7.5$, $\Gamma=1.63$, and $\alpha=0.05$, showing the first and third Fiske steps superimposed on the experimental data (dots). Although the value of the field below the critical value $\Gamma=2$ gives rise in the experimental data to a maximum amplitude of the steps much below that predicted by the theory, we see that the relative position of the resonances and their dynamical resistance is close to that predicted by our model. In (b) we see the current-voltage characteristic of the inline junction of Fig. 8, also showing the first and third Fiske steps. The current-voltage characteristic in this case was fitted for $\alpha=0.1$ and $\Gamma=1.95$.

The characteristics of Fig. 9 also give more direct evidence in favor of the conjecture expressed above that, for a given junction length, when the mode frequency is higher than the plasma frequency, there are more favorable conditions for the application of our model. Indeed, we see that the first steps of Fig. 9, situated below the plasma frequency, have a very irregular shape while the third steps situated just above the plasma frequency have a much more regular shape.

As for the diffraction pattern plots the agreement between

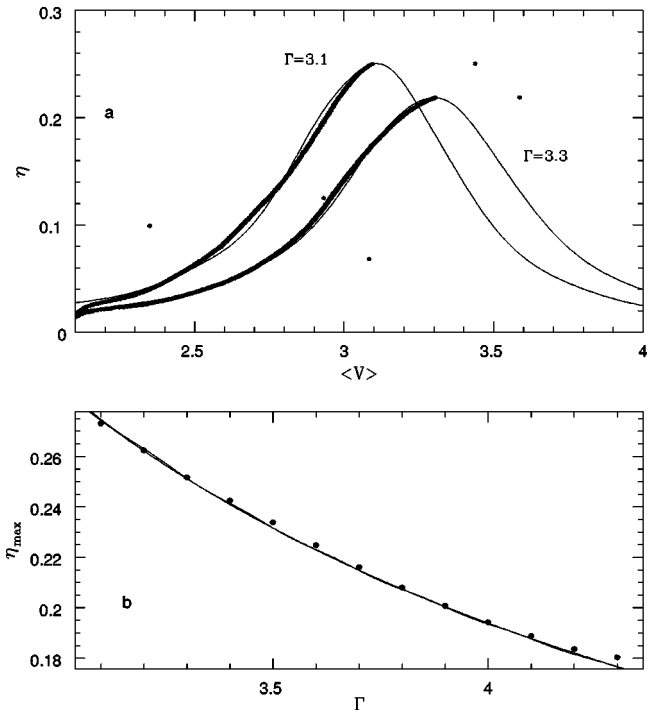

FIG. 10. (a) The experimental data and the theoretical [Eq. (12)] current-voltage characteristic of the Eck step for two values of the applied magnetic field (Γ). (b) The dependence of the maximum current height of the Eck step upon the external magnetic field. The solid line is obtained from Eq. (12), for a loss factor $\alpha=0.68$; note that on this line we have also superimposed the infinite length approximation obtained from Eq. (13) for a loss parameter $\alpha=0.84$.

theoretical and experimental *I-V* curves gets better for higher values of the field. It is worth noting that in all the cases of Figs. 6–8, the value of the damping parameter α giving the best fit to the data was of the same order of magnitude (in the worst case within a factor of 2) of the value that we evaluated from the quasiparticle conductance in the voltage region where the FS's were located. We show now data relative to the appearance of the Eck step for which very good agreement with the theoretical limit $l\rightarrow\infty$ is obtained.

In Fig. 10(a) we report the fittings of the *I-V* curves of the Eck step of an in-line junction with length $l=15$ obtained for two different values of the applied magnetic field. The fittings were obtained from Eq. (12) only setting properly the voltage and scale normalizations and a dissipation factor, respectively, $\alpha=0.46$ and $\alpha=0.52$. These values of the dissipation factor, more than one order of magnitude above those used for the Fiske steps, are reasonable because the ES appears in a region of the current-voltage characteristic where the the quasiparticle resistance of our junctions bends up and a linear constant value becomes a very rough approximation. However, even in this case the values that we obtained from the fits were of the same order of magnitude compared to those measured from the dynamical resistance of the quasiparticle branch. For Fig. 10(a), as for Fig. 5, the background quasiparticle current was subtracted. We note, however, that the position of the maximum of the Eck step does not depend upon the value of the fitting parameter α and therefore Fig. 10(a) also shows (like Fig. 5) that the experimentally observed voltage position of the maximum of the Eck step is equal to the value of the external field.

In Fig. 10(b) we show the dependence of the maximum height of the Eck step upon the external magnetic field as observed in the experiments (dots) and predicted by the theory (lines). In particular, the solid line is obtained from Eq. (12) for a junction length $l=15$, $\alpha=0.68$ while another line obtained from Eq. (13) for an infinitely long junction, for the same value of the applied magnetic field and for $\alpha=0.84$, is almost superimposed on the previous one.

The smooth and continuous ES reported in our figures is observed only when the value of the external magnetic field is driving the resonances in a region of the *I-V* curve with a higher dissipation. It is worth noting that the picture observed in the experiments is very much like that expected from theory and numerical simulations. When increasing the value of the field it becomes difficult to define the spacing between the high-order Fiske modes until the point in which they appear like a single resonance. Considering that this phenomenon takes place for high voltages (and therefore high-order Fiske modes) it is not surprising that the resonance can also be described by the model of Eck, Scalapino, and Taylor[8] [our Eq. (13)] obtained for a junction of infinite length: when the order of the step increases the wavelength of the cavity oscillations decreases and we naturally move toward the limit in which the length of the junction can be considered as infinite. Also, the pictures observed through the simulations clearly show the traveling-wave nature of the linear waves.

We note that the step reported in Fig. 5 and Fig. 10(a) has a very clear resonant nature. It is possible that, for values of the magnetic field close to the threshold for the appearance of the stable Fiske modes ($\Gamma=2$), other kinds of structures may appear in the current-voltage characteristics of the long junctions. These structures that have much the shape of a linear branch in the current-voltage characteristic[11] are likely generated by the average increasing of the velocity of the fluxons when these are not tightly packed together by the external field.[12] These displaced linear slope (or resistive branches) structures, however, appear only in very limited regions of the parameter space and are definitely not useful for devices applications.

As far as concerns the internal dynamics of the junctions during the dynamical state generating the ES and the measurable features displayed in Fig. 10 we note that, since we have obtained a straightforward fit by Eq. (12) and Eq. (13), we expect that the dynamics follow conditions imposed for the derivation of these equations. The ES can be viewed as a ''continuous'' sequence of Fiske steps, generated by the same physical mechanism, i.e.,''linear,'' small amplitude-wave interactions with the Josephson effect. We note that the ES is not a peculiarity of the long junctions as it can be observed in short junctions as well.

V. CONCLUSIONS

We have reported on the extension of theories explaining the appearance of magnetic-field-induced current singularities in Josephson junctions to the case of junctions whose length is not small compared to the Josephson penetration depth. We have shown that this extension includes as a limiting case the result of Eck, Scalapino, and Taylor[8] for the infinitely long junction approximation. The necessary condi-

tion for the applicability of our model, i.e., complete field penetration above the critical value $\Gamma = 2$, is always obeyed in the experiments on junctions of both overlap and in-line geometry where regular current modulations can be observed only above this threshold value. Also, very good agreement is found for the current amplitude of the resonances for $\Gamma \gg 2$ and for the infinite junction approximation.

There are several aspects of our work that could be useful both from the fundamental and from the applied point of view. It has been shown, for example, that the linearized cavity wave analysis may explain several phase-locking phenomena between magnetically coupled Josephson junctions[13] and the same kind of analysis has provided detailed information for the phase locking of a single junction to an external rf drive.[14] From the fittings of the current-voltage characteristics and from the singularity modulations one can estimate the normalized length of the junction, a parameter that is usually extracted from the diffraction pattern of small-area junctions fabricated in the same run and having the same critical current density. This peculiarity could be relevant when working with long high-temperature superconductor junctions[15] or complex systems of coupled junctions with inhomogeneous critical current densities.[2]

Also, after the results[16] which showed that extended Josephson structures could be used as millimeter- and submillimeter-wave oscillators when biased on the Eck step, a number of devices[17,18] and stripline configurations[19] have been proposed and investigated, taking as an essential ingredient of the working principles a dc-bias point on this singularity. It is clear that, for device applications, an analytically defined current-voltage characteristic can turn out to be very useful. We have evaluated quantitatively in terms of the dissipative parameter what the values are that lead to the disappearance of Fiske modes and to the appearance of a single smooth resonance. Our results suggest that moderately shunted long junction oscillators could display the ES over a broader range of frequency and therefore supplying a more stable bias point for broader frequency ranges.

Moreover, we recall that the Fiske steps of large-area junctions are interesting because their dc current levels, higher than those of the small-area junctions, can provide narrow-linewidth radiation[10] with a better stability with respect to fluxon oscillations. The above systematic characterization could be very useful for future developments of possible high-frequency devices.

ACKNOWLEDGMENTS

The junctions used for the experiments were fabricated by M. Cirillo and F. Santucci at the IESS-CNR, Rome. We thank the members of the low-T_c superconductivity group in that laboratory (P. Carelli, M. G. Castellano, R. Leoni, and G. Torrioli) for access to the clean room facility and equipment. Parts of this work were performed under the auspices of the U.S. Department of Energy.

*Permanent address: Department of Physics, The Technical University of Denmark, DK-2800 Lyngby, Denmark.

[1] R. D. Parmentier, in *The New Superconducting Electronics*, edited by H. Weinstock and R. W. Ralston (Kluwer, Dordrecht, 1993), pp. 221–248.

[2] A. Barone and G. Paternò, *Physics and Applications of the Josephson Effect* (Wiley, New York, 1982).

[3] D. W. McLaughlin and A. C. Scott, Phys. Rev. A **18**, 1652 (1978).

[4] N. F. Pedersen and D. Welner, Phys. Rev. B **29**, 2551 (1984).

[5] S. Pagano, M. P. Soerensen, R. D. Parmentier, P. L. Christiansen, O. Skovgaard, J. Mygind, N. F. Pedersen, and M. R. Samuelsen, Phys. Rev. B **33**, 174 (1986).

[6] M. Cirillo, T. Doderer, S. G. Lachenmann, F. Santucci, and N. Grønbech-Jensen, Phys. Rev. B **56**, 11 889 (1997).

[7] I. O. Kulik, JETP Lett. **2**, 84 (1965); Zh. Tekh. Fiz. **37**, 157 (1967) [Sov. Phys. Tech. Phys. **12**, 111 (1967)].

[8] R. E. Eck, D. J. Scalapino, and B. N. Taylor, Phys. Rev. Lett. **13**, 15 (1964).

[9] J. A. Blackburn, J. D. Leslie, and H. J. Smith, J. Appl. Phys. **42**, 1047 (1971).

[10] M. Cirillo, F. Santucci, P. Carelli, M. G. Castellano, and R. Leoni, J. Appl. Phys. **73**, 8637 (1993).

[11] S. Pace and U. Gambardella, J. Low Temp. Phys. **62**, 197 (1986); A. V. Ustinov, H. Kohlstedt, and P. Henne, Phys. Rev. Lett. **77**, 3617 (1997).

[12] M. Cirillo, B. H. Larsen, A. V. Ustinov, V. Merlo, V. A. Oboznov, and R. Leoni, Phys. Lett. A **183**, 383 (1993).

[13] N. Grønbech-Jensen, J. A. Blackburn, and M. R. Samuelsen, Phys. Rev. B **53**, 12 364 (1996).

[14] N. Grønbech-Jensen and M. Cirillo, Phys. Lett. B **50**, 12 851 (1994); N. Grønbech-Jensen, P. S. Lomdahl, and M. Cirillo, *ibid.* **51**, 11 690 (1995).

[15] D. Winkler, Y. M. Zhang, P. Å. Nilsson, E. A. Stepantsov, and T. Claeson, Phys. Rev. Lett. **72**, 1260 (1994).

[16] T. Nagatsuma, K. Enpuku, F. Irie, and K. Yoshida, J. Appl. Phys. **54**, 3302 (1983).

[17] V. P. Koshelets, A. V. Shchukin, S. V. Shitov, and L. V. Filippenko, IEEE Trans. Appl. Supercond. **3**, 2524 (1993).

[18] A. V. Ustinov, J. Mygind, and V. A. Oboznov, J. Appl. Phys. **72**, 1203 (1992).

[19] Y. M. Zhang and D. Winkler, IEEE Trans. Microwave Theory Tech. **4**, 726 (1994).